A variant conferring cofactor-dependent assembly of *Escherichia coli* dimethylsulfoxide reductase

Huipo Tang, Richard A. Rothery, Joel H. Weiner *

Department of Biochemistry, Membrane Protein Disease Research Group, University of Alberta, Edmonton, Alberta, Canada T6G 2H7

A B S T R A C T

We have investigated the final steps of complex iron–sulfur molybdoenzyme (CISM) maturation using *Escherichia coli* DMSO reductase (DmsABC) as a model system. The catalytic subunit of this enzyme, DmsA, contains an iron–sulfur cluster (FS0) and a molybdo-bis(pyranopterin guanine dinucleotide) cofactor (Mo-bisPGD). We have identified a variant of DmsA (Cys59Ser) that renders enzyme maturation sensitive to molybdenum cofactor availability. DmsA-Cys59 is a ligand to the FS0 [4Fe–4S] cluster. In the presence of trace amounts of molybdate, the Cys59Ser variant assembles normally to the cytoplasmic membrane and supports respiratory growth on DMSO, although the ground state of FS0 as determined by EPR is converted from high-spin ($S = 3/2$) to low-spin ($S = 1/2$). In the presence of the molybdenum antagonist tungstate, wild-type DmsABC lacks Mo-bisPGD, but is translocated via the *Tat* translocon and assembles on the periplasmic side of the membrane as an apoenzyme. The Cys59Ser variant cannot overcome the dual insults of amino acid substitution *plus* lack of Mo-bisPGD, leading to degradation of the DmsABC subunits. This indicates that the cofactor can serve as a chemical chaperone to mitigate the destabilizing effects of alteration of the FS0 cluster. These results provide insights into the role of the Mo–bisPGD–protein interaction in stabilizing the tertiary structure of DmsA during enzyme maturation.

© 2013 Published by Elsevier B.V.

1. Introduction

Members of the bacterial complex iron sulfur molybdoenzyme (CISM) family play critical roles in global geochemical cycles and bacterial metabolic diversity, contributing to the ability of prokaryotes to exploit the plethora of ecological niches on Earth [1,2]. Archetypal members comprise a catalytic subunit containing a molybdo-bis(pyranopterin guanine dinucleotide) cofactor (Mo-bisPGD) and a single [4Fe–4S] cluster known as FS0, an electron-transfer subunit that typically contains four [4Fe–4S] clusters, and a membrane–anchor subunit that can contain zero or two *b*-type hemes. These enzymes support metabolic diversity by coupling redox reactions of soluble substrates at the Mo-bisPGD to the membrane-intrinsic quinone pool via a ~70 Å to ~100 Å long multi-cofactor electron-transfer relay and a quinone binding site located in the membrane–anchor subunit [3–5]. The diversity of soluble substrate specificity is derived from the utility of the Mo-bisPGD in catalyzing redox reactions ranging from the oxidation of formate to CO_2 ($E_{m,7} = -432$ mV) to the reduction of nitrate to nitrite ($E_{m,7} = +420$ mV) [6]. While delineation of the Mo-bisPGD biosynthetic pathway is largely complete [7], the final steps of its insertion into the respective enzymes remain poorly understood, and involve a system-specific chaperone referred to as a redox enzyme maturation protein (REMP) [8].

Maturation of two *Escherichia coli* CISM enzymes has been studied in detail: nitrate reductase A (NarGHI) and DMSO reductase (DmsABC) [2,8–10]. Importantly, NarGHI is assembled to the inner surface of the cytoplasmic membrane, whereas DmsABC is assembled to the outer surface, with the DmsAB subunits being translocated across the membrane by the *Tat* translocon [11,12]. In both cases, a REMP, NarJ or DmsD, is required to facilitate both Mo–bisPGD insertion and correct targeting of the enzyme to the cytoplasmic membrane. In the case of NarGHI, NarJ appears to hold the apomolybdoenzyme in a cofactor-binding competent conformation during the final stages of maturation [13], and appears to do this by interacting with two sites on the NarG subunit: the approximately 50 amino acid pseudo-*Tat* leader and a second as-yet unidentified site elsewhere on the subunit [14–16]. In the case of DmsABC, a *Tat*-leader at the N-terminus of DmsA directs the fully-folded cofactor-containing DmsAB catalytic dimer to the periplasmic compartment by binding DmsD and being directed to the *Tat* translocon, where it associates with the membrane intrinsic DmsC subunit to form an active heterotrimer. Support for a role of DmsD in cofactor insertion comes from the observation that if the DmsA *Tat* leader

is replaced with that from the periplasmic trimethylamine-*N*-oxide reductase (TorA), DmsABC assembles to the membrane in its apomolybdo form [17], indicating a role for the cognate REMP in both targeting and cofactor insertion.

An aspect of CISM maturation that has received little attention is the interplay between FS0 assembly and Mo-bisPGD insertion. In the case of NarGHI, mutation of NarG-His50 to Ser results in assembly of an enzyme lacking both FS0 and Mo-bisPGD [18]. Mutants of the FS0-coordinating Cys motif in DmsA that eliminate its detection by EPR also eliminate insertion of Mo-bisPGD [19]. These observations indicate that correct assembly of FS0 is a prerequisite for Mo-bisPGD insertion; specifically that correct folding of the FS0-binding domain of the CISM catalytic subunit, known as Domain I [1], is a prerequisite for cofactor insertion. In the absence of insertion-competent cofactor, for example in cells grown in the presence of the molybdenum-antagonist tungstate or in cells bearing a mutation in the cofactor biosynthetic pathway, both enzymes are able to bypass the cofactor-insertion step and assemble to the cytoplasmic membrane in their respective apomolybdo forms [2,20–22]. These observations prompted us to address the role of the FS0-pyranopterin interplay in the assembly of DmsABC in a variant with an altered FS0 cluster that destabilizes DmsA, DmsA-Cys59Ser. One intriguing aspect of this is that the estimated ~30 contacts [23] between the Mo-bisPGD and the protein may be able to play a role in stabilizing the structure of DmsA during enzyme maturation. In this paper, we demonstrate that Mo-bisPGD can act as a chemical chaperone [24] to stabilize a functional DmsA-Cys59Ser variant.

2. Materials and methods

2.1. Bacterial strains and plasmids

The *E. coli* strains and plasmids used in this study are listed in Table 1. *E. coli* strains HB101 and TOPP2 each have a wild-type chromosomal copy of the *dmsABC* operon, resulting in accumulation of both wild-type and variant DmsABC [25,26]. In *E. coli* DSS301, the chromosomal copy of the *dmsABC* operon is replaced with a kanamycin resistance cartridge [27]. Plasmid pDMS160 bears the wild-type *dmsABC* operon behind an *fnr*-dependent promoter [25]. pDMS160-C59S has a point mutation that changes Cys59 of DmsA to a Ser [26]. As a control, the same vector lacking the *dmsABC* operon (pBR322) was used.

2.2. Growth of cells and preparation of membrane vesicles

Cells were grown anaerobically in 9 L or 19 L batch cultures at 37 °C for 24 h (TOPP2 and DSS301) or 48 h (HB101) on a glycerol–fumarate minimal medium [28]. The growth medium was supplemented with either molybdate or tungstate (concentrations used are given in the individual table and figure legends). Where appropriate, ampicillin and kanamycin were added to a final concentration of 100 µg mL^{-1} and

Table 1
Bacterial strains and plasmids.

	Description
Strains	
HB101	*supE44 hsd20* (r$_B^-$ m$_B^-$) *recA13 ara-14 proA2 lacY1 galK2 rpsL20 xyl-5 mtl-1*
DSS301	TG1, *kan*^{R} Δ*dmsABC*
TOPP2	rif^R F′ *proAB*, lacI^{q}ZΔM15 Tn10 (tet^R)
F36	HB101, *moeB*
RK5209	Δ*lacU169 araD139 rpsL gyrA non mod241::Mu cts*
Plasmids	
pDMS160	pBR322 Amp^R (*dmsABC*)$^+$
pDMS160C59S	pBR322 Amp^R (*dmsA*^{Cys59Ser}*BC*)$^+$

50 µg mL^{-1}. Cells were harvested, and washed in 100 mM MOPS and 5 mM EDTA (pH7.0). Membranes were prepared by cell lysis using a French pressure cell or an Avestin micro-fluidizer, followed by differential centrifugation as previously described [25,29]. Respiratory growth on DMSO was evaluated using a Klett–Summerson spectrophotometer and 160 mL side-arm Erlenmeyer flasks as previously described [20,25].

2.3. Purification of DmsABC

Membranes were detergent-solubilized with 1% *n*-dodecy-β-D-maltoside and enzyme purification was performed as previously described [19].

2.4. Protein assays

Protein concentrations were determined by the Lowry method [30], modified by the inclusion of 1% (wt/vol) sodium dodecyl sulfate in the incubation mixture to solubilize membrane proteins [31].

2.5. Immunoblot analysis of DmsABC content in cell membranes

Proteins from membrane vesicles were separated on a 12% SDS-PAGE gel and then blotted onto nitrocellulose. Antibodies to DmsA and DmsB were used for Western blot analysis. DmsA and DmsB were detected using the GE Healthcare chemiluminescence system and goat anti-rabbit IgG horseradish peroxidase conjugate [32].

2.6. Preparation of fluorescent pyranopterin derivatives

The presence of pyranopterin in membrane vesicles was assayed by acid denaturation followed by I$_2$ and KI oxidation to produce an extract that contained the Form A fluorescent derivative of pyranopterin that will be referred herein to as a "Form A extract" [21,33]. 20 mg of membrane protein was used as starting material. Prior to recording fluorescence spectra using a Perkin-Elmer LS-50B luminescence spectrometer, small aliquots (200 µL) of the acid-denatured iodine-oxidized extract were added to 3 mL of 1 M NH$_4$OH in a fluorescence cuvette. Excitation spectra were recorded from 240–420 nm (emission at 448 nm). Emission spectra were recorded from 410–520 nm (excitation at 397 nm).

2.7. Quantitation of quinol-binding to DmsABC

Fluorescence quench titrations were used to quantitate membrane-bound DmsABC by measuring the concentration of 2-*n*-heptyl-4-hydroxyquinoline-*N*-oxide (HOQNO) binding sites [19,34]. HOQNO is a menaquinol analog that binds to the quinol-binding site of DmsC with 1:1 stoichiometry and high affinity (K_d ~ 7 nM). Quenching of HOQNO fluorescence was used to estimate the concentration of DmsC and thus DmsABC in the membrane samples [35,36]. HOQNO fluorescence was recorded using a Perkin-Elmer LS-50B luminescence spectrophotometer using an excitation wavelength of 341 nm and an emission wavelength of 479 nm. Aliquots of 0.1 mM HOQNO were added to membrane samples at a protein concentration of 1 mg mL^{-1}. The concentration of DmsABC is equal to the concentration of HOQNO immediately preceding the rise in fluorescence [37].

2.8. Enzyme activity assay

Enzyme activity was determined as the rate of trimethylamine-*N*-oxide (TMAO)-dependent oxidation of dithionite-reduced benzyl viologen (BV) as previously described [38]. The extinction coefficient for BV is 7.4 mM^{-1} cm^{-1}.

2.9. Electron paramagnetic resonance (EPR) spectroscopy

Reduced samples were prepared by anaerobic incubation of purified DmsABC or membrane samples with 5 mM (final concentration) sodium dithionite for 5 min at room temperature. Oxidized samples were prepared by mixing with air. Redox titrations were carried out anaerobically at 25 °C under argon in the presence of redox dyes as previously described [29,39,41]. The dyes added to a final concentration of 50 μM were quinhydrone, 2,6-dichloroindophenol, 1,2-naphthoquinone, toluylene blue, phenazine methosulfate, thionine, duroquinone, methylene blue, resorufin, indigotrisulfonate, indigodisulfonate, anthraquinone-2-sulfonic acid, phenosafranine, benzyl viologen, and methyl viologen. All samples were prepared in 3 mm internal diameter quartz EPR tubes, and were rapidly frozen in liquid nitrogen-chilled ethanol and stored under liquid nitrogen until use. EPR spectra were recorded using a Bruker ELEXSYS E500 spectrometer equipped with a Bruker SHQE cavity and an Oxford Instruments ESR-900 flowing helium cryostat, or with a Bruker ESP300E equipped with a TE_{102} cavity and with either a ESR-900 cryostat or a Bruker liquid nitrogen evaporating cryostat was used (Bruker ER4111VT). Instrument conditions and temperatures used were are described in the figure legends. Microwave power saturation data were analyzed as previously described [39,41].

3. Results

3.1. DmsA-Cys59 coordinates the FS0 cluster of DmsA

The electron-transfer relay connecting the menaquinol binding site within the DmsC subunit to the Mo-bisPGD cofactor of DmsA comprises four [4Fe–4S] clusters located in the DmsB subunit and the FS0 [4Fe–4S] cluster of DmsA that is close to the proximal pyranopterin of the cofactor [1,19] (Fig. 1A). Fig. 1B shows the predicted protein structure surrounding the FS0 cluster with DmsA-Cys59 providing one of its four sulfur ligands [19]. The work presented herein addresses the effect of a DmsA-Cys59Ser variant in rendering assembly of the DmsABC complex (Fig. 1B) sensitive to the availability of the Mo-bisPGD cofactor.

3.2. Assembly of the DmsA-Cys59Ser variant is impaired by growth in the presence of tungstate

Membrane fractions from E. coli DSS301 cells (ΔdmsABC) expressing either wild-type enzyme or the DmsA-Cys59Ser variant in the presence of either molybdate or tungstate were subjected to immunoblot analysis (Fig. 2). While growth in the presence of the molybdenum antagonist tungstate has no demonstrable effect on the assembly of wild-type enzyme, it clearly diminishes assembly of the DmsA-Cys59Ser variant. Given the large number of contacts between the Mo-bisPGD and the protein [23], this observation is consistent with the Mo-bisPGD acting as a chemical chaperone [24] during maturation of the DmsA-Cys59Ser variant.

3.3. The DmsA-Cys59Ser variant supports respiratory growth on DMSO

Fig. 3A confirms that, as reported previously, the DmsA-Cys59Ser variant supports respiratory growth on DMSO in DSS301, a ΔdmsABC mutant [26]. As expected, this growth is inhibited by the molybdenum antagonist tungstate. Similar behavior is exhibited when the wild-type HB101 strain is used (Fig. 3B), with the only significant difference being the slower overall growth rate exhibited by this strain. As E. coli HB101 expresses higher levels of DmsABC in comparison with DSS301, membrane preparations for fluorescence and EPR studies were prepared from HB101 cells grown anaerobically on a glycerol–fumarate minimal medium [25,28].
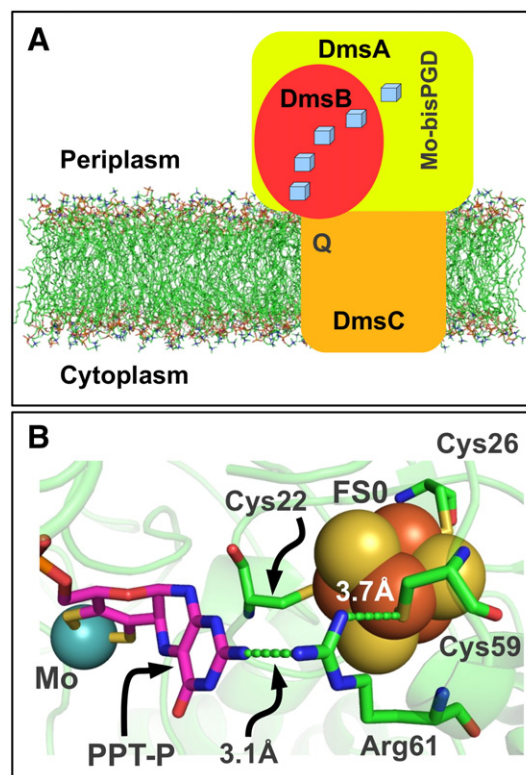

Fig. 1. Electron-transfer relay architecture and predicted DmsA structure around FS0. (A) Overall topology and electron-transfer relay of DmsABC in the cytoplasmic membrane with the DmsAB catalytic dimer attached to the periplasmic side of DmsC. The approximate position of the quinone binding site is indicated as a "Q" in the panel, and blue cubes represent the five [4Fe-4S] clusters of DmsABC. (B) Structural model of DmsA in the vicinity of FS0 was generated as previously described [19]. The predicted position of the DmsA-Cys59 is shown. The distances shown are arbitrary. PPT-P, proximal pyranopterin.
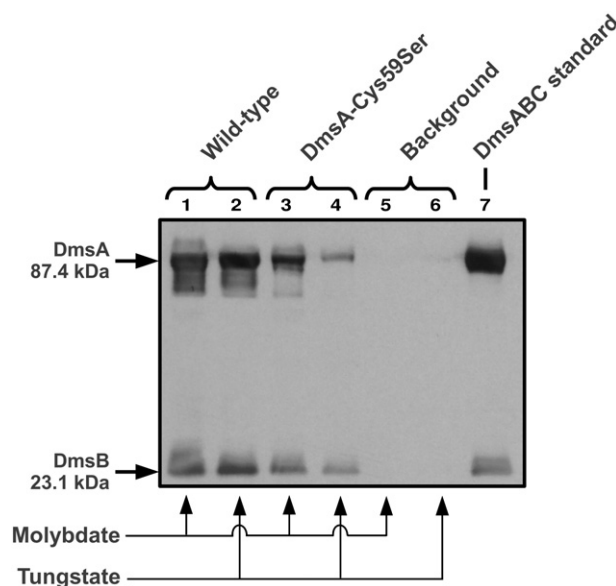

Fig. 2. Tungstate decreases enzyme maturation in a DmsA-Cys59Ser variant. Western blot of membrane samples run on a 10% SDS-polyacrylamide gel with 45 μg (total protein) of the following membrane samples: *lane 1*, E. coli DSS301/pDMS160 in the presence of 5 μM sodium molybdate; *lane 2*, E. coli DSS301/pDMS160 in the presence of 100 μM sodium tungstate; *lane 3*, E. coli DSS301/pDMS160C59S in the presence of 5 μM sodium molybdate; *lane 4*, E. coli DSS301/pDMS160C59S in the presence of 100 μM sodium tungstate; *lane 5*, E. coli DSS301/pBR322 in the presence of 5 μM sodium molybdate; *lane 6*, E. coli DSS301/pBR322 in the presence of 100 μM sodium molybdate; *lane 7*, purified DmsABC standard.
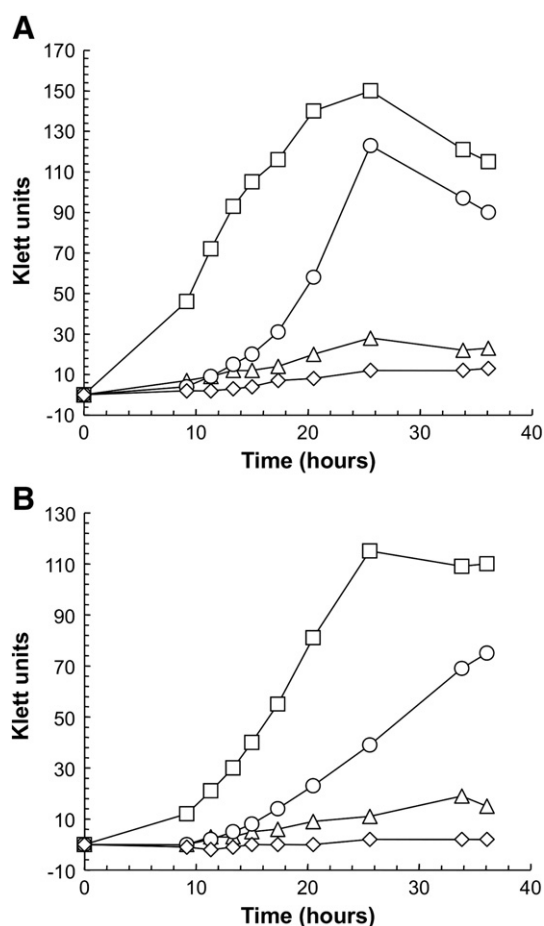
A

B

Fig. 3. Effect of tungstate on respiratory growth on DMSO. (A) Growth of *E. coli* DSS301. (B) Growth of *E. coli* HB101. *Squares* — *E. coli* HB101/pDMS160 in the absence of tungstate. *Circles* — *E. coli* HB101/pDMS160C59S in the absence of tungstate. *Triangles* — *E. coli* HB101/pDMS160 in the presence of 10 mM tungstate. *Diamonds* — *E. coli* HB101/pDMS160C59S in the presence of 10 mM tungstate. Cell growth was measured with a Klett–Summerson spectrophotometer equipped with a number 66 filter.

3.4. Tungstate inhibits maturation of the entire complex in the DmsA-Cys59Ser variant

The pyranopterin cofactor cannot be assayed directly and an oxidized fluorescent derivative Form A is used as a measure of cofactor insertion. Fig. 4A shows the effect of tungstate on the relative amounts of Form A pyranopterin derivative in membrane fractions derived from the HB101 strain. As expected (Fig. 4Ai, Aii), a significant amount of cofactor is detected in membranes prepared from cells grown in the presence of molybdate [20,21]. The level of Form A derivative prepared from the DmsA-Cys59Ser variant is comparable to that obtained from wild-type DmsABC (*cf.* Fig. 4Ai and Aii).

As expected, growth in the presence of tungstate decreases the amount of cofactor released from membranes containing wild-type or DmsA-Cys59Ser enzyme (Fig. 4Aiii). We have previously demonstrated that in both DmsABC and NarGHI, growth in the presence of tungstate has little or no effect on the total amount of enzyme assembled to the cytoplasmic membrane [20,21]. Overall, analyses of Form A extracts from membranes are consistent with the immunoblot analysis presented in Fig. 2.

It is important to correlate cofactor detection by assaying Form A extracts with the overall assembly of the enzyme. Fluorescence quench titrations using the chromophore HOQNO allow the concentration of DmsABC-associated quinol binding sites to be measured in membrane samples [34,37]. Fig. 4B shows titrations performed with HB101 membranes containing wild-type, DmsA-Cys59Ser variant
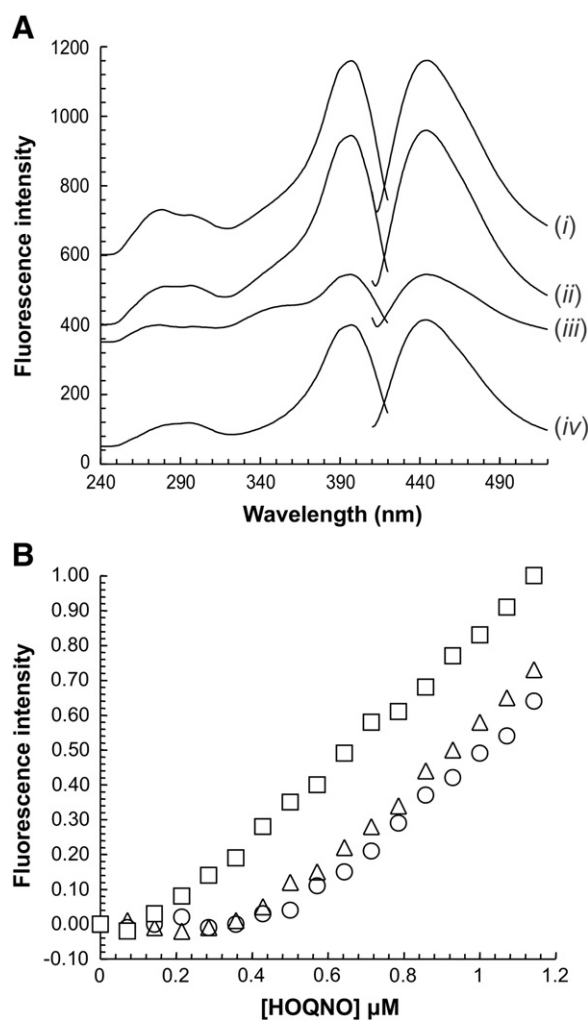
A

B

Fig. 4. Loss of cofactor inhibits assembly of the DmsA-Cys59Ser variant. (A) Fluorescence spectra of Form A extracts of membranes from cells grown in the presence of molybdate and tungstate. (*i*) Spectra of membranes from *E. coli* HB101/pDMS160 cells expressing wild-type DmsABC grown in the presence of 5 μM molybdate; (*ii*) spectra of membranes from *E. coli* HB101/pDMS160C59S cells in the presence of 5 μM molybdate; (*iii*) spectra of membranes from *E. coli* HB101/pDMS160C59S cells grown in the presence of 15 mM tungstate; and (*iv*) difference spectra of (*ii*) minus (*iii*). 10 mg of membrane protein was used as starting material. Spectra were recorded under the following conditions: excitation spectra (left of panel A), scanned from 240–420 nm with an emission wavelength of 442 nm; emission spectra (right of panel A), scanned from 410–520 nm with an excitation wavelength of 395 nm. (B) Quantitation by fluorescence quench titration of quinol binding sites in membranes containing DmsABC or DmsA-Cys59Ser variant enzyme. *Circles* — membranes containing wild-type enzyme; *triangles* — membranes from cells expressing the DmsA-Cys59Ser variant in the presence of 5 μM molybdate; *squares* — membranes from cells expressing the DmsA-Cys59Ser variant in the presence of 15 mM tungstate. Enzyme concentrations were estimated from the X-intercepts of the plots to be 0.54, 0.48, and 0.17 nmol (mg membrane protein)$^{-1}$ for the wild-type, DmsA-Cys59Ser variant (molybdate), and the DmsA-Cys59Ser variant (tungstate) membranes, respectively. Titrations were carried out at a protein concentration of 1 mg mL^{-1}.

(molybdate) and DmsA-Cys59Ser variant (tungstate) enzymes, yielding HOQNO binding site concentrations of 0.54, 0.48, and 0.17 nmol (mg membrane protein)$^{-1}$, respectively. Growth in the presence of tungstate has no effect on the amount of HOQNO binding sites detected in membranes containing DmsABC accumulated to the cytoplasmic membrane as assayed by immunoblot (Fig. 2) and fluorescence quench titration (data not shown). Essentially similar results were obtained using the alternative wild-type strain *E. coli* TOPP2 (data not shown). These results demonstrate that in the DmsA-Cys59Ser variant there is a correlation between a decreased level of DmsA and DmsB subunits detected by immunoblot (Fig. 2) with a decreased level of Form A derivative released from membrane samples (Fig. 4A) and a decreased

concentration of detectable HOQNO binding sites. Critically, this suggests a coordination of the maturation of all three subunits of the holoenzyme.

3.5. EPR characterization of the DmsA-Cys59Ser variant

Fig. 5 shows EPR spectra recorded at 12 K of dithionite-reduced membranes containing wild-type DmsABC and the DmsA-Cys59Ser variant expressed in the presence and absence of tungstate. As expected, the spectrum of membranes containing wild-type DmsABC (Fig. 5a) resembles those previously published [29,38]. It arises from the paramagnetic [4Fe–4S] clusters located in the DmsB subunit and has well-defined peaks at around $g = 2.05$, 2.02, and 1.99; and well defined troughs at $g = 1.92$ and 1.88 [29,38]. Because the membranes were derived from cells that were grown anaerobically on fumarate, there is a minor contribution to the spectrum from the [Fe–S] clusters of fumarate reductase [25,26,29]. Specifically, fumarate reductase contributes to the peak at $g = 2.02$ and to the trough at $g = 1.92$. Spectra of membranes containing the DmsA-Cys59Ser variant (Fig. 5b) resemble those of membranes containing the wild-type enzyme, but have a more pronounced peak at $g = 2.05$ (indicated by the position of the arrows in Fig. 5). Spectra of membranes containing the DmsA-Cys59Ser variant obtained from cells grown in the presence of tungstate are greatly diminished in intensity and more closely resemble those observed for membranes containing fumarate reductase (Fig. 5c) [34]. When the spectrum of membranes grown in the presence of tungstate is subtracted from the spectrum of membranes grown in the presence of molybdate, the result resembles that of purified enzyme [38] with the caveat that it has a more pronounced peak at $g = 2.05$ (Fig. 5(c), see below).
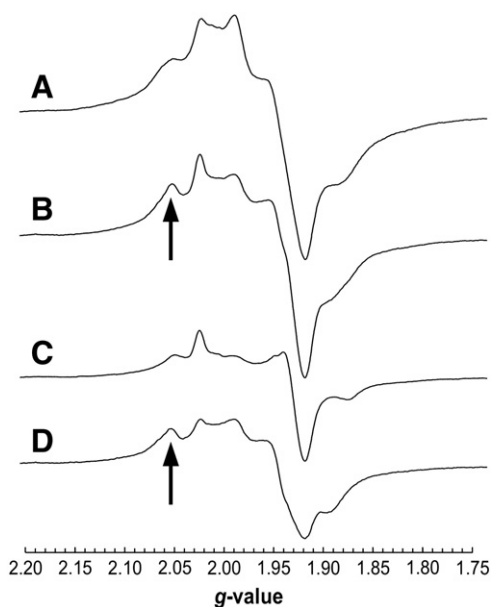

Fig. 5. Effect of tungstate on assembly of the DmsA-Cys59Ser variant determined by EPR spectroscopy of its clusters. All spectra are of dithionite (5 mM) reduced samples prepared as described in the Materials and methods section. (a) Spectrum of HB101/pDMS160 membranes from cells grown on molybdate-supplemented medium. (b) Spectrum of HB101/pDMS160C59S membranes from cells grown on molybdate-supplemented medium. (c) Spectrum of HB101/pDMS160C59S membranes grown on tungstate-supplemented medium (15 mM). (d) Difference spectrum of (b) minus 0.8× (c). EPR spectra were recorded under the following instrument conditions: temperature, 12 K; microwave power, 20 mW; microwave frequency, 9.47 GHz; modulation amplitude, 10 G_{pp} at 100 KHz. Spectra were normalized to a protein concentration of 30 mg mL^{-1}. Vertical arrows indicate the increased intensity of the $g = 2.05$ peak in spectra of samples containing the DmsA-Cys59Ser variant.

3.6. Characterization of the FS0 cluster of the DmsA-Cys59Ser variant

Because DmsA-Cys59 is a ligand to the FS0 cluster and this cluster is close to the Mo-bisPGD (Fig. 1B), it is important to evaluate any effects of a Cys59Ser substitution on the electrochemistry of both the cluster and the Mo center. Fig. 6A shows a comparison of redox-poised EPR spectra recorded at 75 K, demonstrating that the Mo(V)
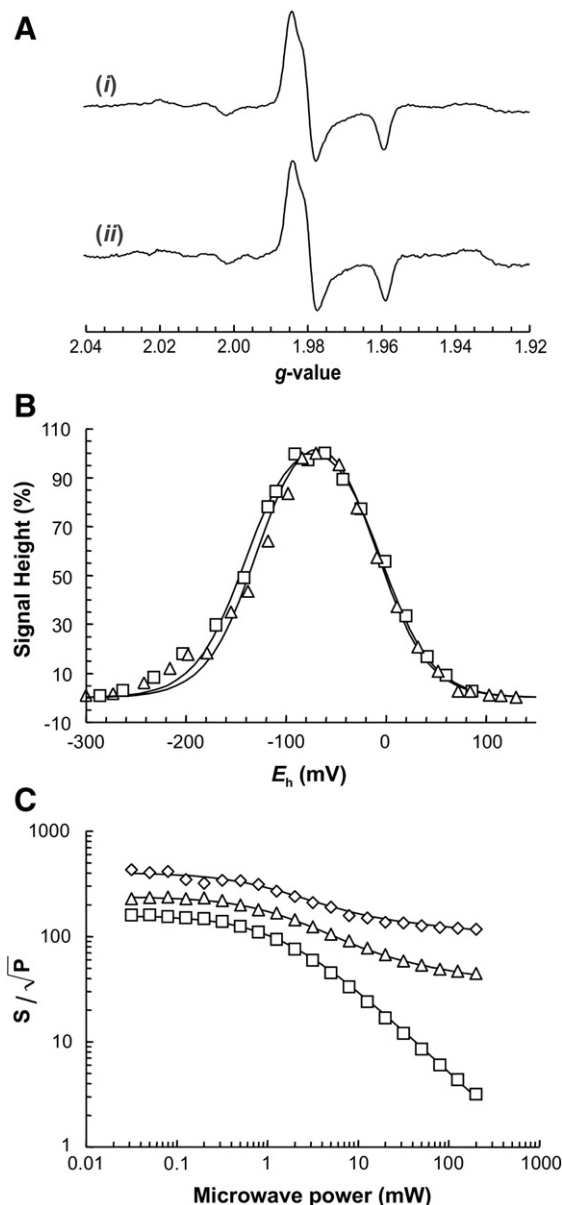

Fig. 6. EPR characterization of Mo-bisPGD in the DmsA-Cys59Ser variant. (A). Mo(V) EPR spectra of membranes containing wild-type (**i**) and DmsA-Cys59Ser variant enzyme (**ii**). Samples were redox-poised as described in the Materials and methods section at −91 mV (*i*) and −98 mV (*ii*). Spectra were recorded with the following EPR parameters: temperature, 75 K, modulation amplitude, 3.8 G_{pp} at 100 KHz; microwave power, 2 mW. (B). Redox titration of the $g = 1.98$ peak-trough of the wild-type and DmsA-Cys59Ser variant Mo(V) signals. *Squares* − wild-type (Mo(V/VI) $E_{m,7} = −5$ mV, Mo(IV/V) $E_{m,7} = −140$ mV). *Triangles* − DmsA-Cys59Ser variant (Mo(V/VI) $E_{m,7} = −10$ mV, Mo(IV/V) $E_{m,7} = −128$ mV). Data were obtained from EPR spectra recorded as described for (A). (C) Microwave power saturation curves for the $g = 1.98$ peak-trough of the DmsA-Cys59Ser variant Mo(V) spectrum of redox-poised samples. *Squares* − $E_h = −29$ mV ($P_{1/2} = 1.4$ mW, $b = 1.6$). *Triangles* − $E_h = −138$ mV ($P_{1/2} = 1.5$ mW, $b = 1.6$, 82%). *Diamonds* − $E_h = −179$ mV ($P_{1/2} = 1.1$ mW, $b = 1.6$, 70%). Percentages indicate the estimated amount of saturable *versus* non-saturable Mo(V). Where appropriate, a non-saturable component with nominal $P_{1/2}$ of 1000 mW was included in the fits. EPR spectra were recorded as described for A, except that the temperature was 30 K and the modulation amplitude was 6G_{pp}.

EPR spectrum of the DmsA-Cys59Ser variant is essentially identical to that of the wild-type. Fig. 6B illustrates redox titrations of Mo for the two enzymes. The wild-type enzyme has reduction potentials ($E_{m,7}$ values) of approximately −5 mV (Mo(VI/V)) and −140 mV (Mo(V/IV)), whereas the DmsA-Cys59Ser variant has reduction potentials of −10 mV (Mo(VI/V)) and −128 mV (Mo(V/IV)). Thus, there is modest 12 mV increase in the Mo(V/IV) reduction potential in the DmsA-Cys59Ser variant compared to the wild-type. A final issue that can be addressed by studying the Mo(V) EPR spectrum is the paramagnetic interaction between it and the reduced form of the FS0 cluster [39]. Fig. 6C shows the change in spin relaxation of the Mo(V) center that occurs as the ambient potential is decreased from −29 mV to −179 mV [1,39]. As the potential is decreased, the proportion of rapidly-relaxing Mo(V) signal increases, and in the

Fig. 7. EPR spectra of the purified DmsA-Cys59Ser variant. (A) EPR spectra recorded in the g = 2.0 region showing oxidized (*i*) and dithionite-reduced (*ii*) wild-type enzyme; and oxidized (*iii*) and reduced (*iv*) DmsA-Cys59Ser variant enzymes. (B) EPR spectra in the low field region showing the spectrum of reduced FS0 with a high-spin ground state (*I*) and the lack of a similar spectrum exhibited by the purified DmsA-Cys59Ser variant.

wild-type enzyme, this phenomenon titrates with an apparent reduction potential of approximately −140 mV [39]. In the case of the DmsA-Cys59Ser variant, an estimated 70% of the observable Mo(V) is slowly-relaxing and thus not interacting with reduced FS0 at a potential of −179 mV, indicating that the reduction potential of FS0 is significantly lower than this value. It was not possible to explore potentials lower than approximately −179 mV using this method, as the intrinsic intensity of the Mo(V) spectrum becomes negligible at lower potentials (Fig. 6B). Unfortunately, FS0 has proven recalcitrant to efforts to directly measure the reduction potential of its high-spin EPR spectrum [19] (see below).

To further investigate the line shape change observed in the low temperature (12 K) EPR spectrum of the reduced DmsA-Cys59Ser variant, we purified it from *E. coli* TOPP2 membranes [19]. Fig. 7 shows representative EPR spectra recorded at 9 K at around g = 2.0 (Fig. 7A) and at around g = 5.0 (Fig. 7B). Reduced spectra at around g = 2.0 confirm the difference between the wild-type and DmsA-Cys59Ser variant observed in HB101 membranes in Fig. 5, with a more pronounced shoulder observed at g = 2.05. Spectra of air oxidized samples (Fig. 7A(i) and A(iii)) indicate that a fraction of FS0 is converted to a [3Fe–4S] cluster in the DmsA-Cys59Ser variant (spectral features comprising a peak at ~g = 2.02 with a peak-trough immediately upfield). Inspection of the spectra of reduced purified samples at around g = 5 reveals that the increased intensity of the g = 2.05 shoulder is correlated with the almost complete elimination of a g = 5.07 signal corresponding to a form of the FS0 cluster with a high-spin S = 3/2 ground state [19]. Based on these observations, it is likely that the DmsA-Cys59Ser substitution changes the ground state of the reduced FS0 from S = 3/2 to S = 1/2.

3.7. Effect of the DmsA-Cys59Ser variant on enzyme activity

In agreement with our previous work [26], the DmsA-Cys59Ser variant is able to support respiratory growth on DMSO (Fig. 3). In order to correlate the observed growth with enzyme activities, we measured normalized enzyme activities corrected for enzyme concentration in *E. coli* TOPP2 membranes determined by fluorescence quench titration. The turnover number of wild-type and DmsA-Cys59 variant enzymes from cells grown in the presence of 5 μM molybdate was 3240 s^{-1} and 3238 s^{-1}, respectively, indicating that these enzymes were both equally effective at reducing substrate and consistent with their ability to support respiratory growth on DMSO. Increasing concentrations of molybdate (up to 10 mM) had no effect on the observed turnover rates. Finally, tungstate eliminated measurable enzyme activity, consistent with it being an effective molybdenum antagonist.

4. Discussion

The results presented herein provide new insights into the interplay between the FS0 cluster and the Mo-bisPGD cofactor during maturation of CISM catalytic subunits. We previously demonstrated in both DmsABC and NarGHI that FS0 assembly into the respective apomolybdoenzymes is a prerequisite for Mo-bisPGD insertion [18,19]. In the present work, we show that in a DmsA-Cys59Ser variant, assembly of the entire complex is dependent on the availability of Mo-bisPGD. This can be understood in the context of hydrogen bond formation between the amino acids of DmsA and the cofactor: there are approximately 30 predicted hydrogen-bonding contacts [23], each of which is likely to stabilize the structure by between 5.7 to 27 kJ mol^{-1} [42,43]. In the wild-type enzyme, absence of cofactor appears to have essentially no effect on the amount of protein assembled to the membrane, presumably due to the large size and inherent stability of DmsA (85.8 kDa; 768 amino acids) within the complex. In the present study, we demonstrate that a combination of a critical point mutation in DmsA and lack of cofactor results in significant
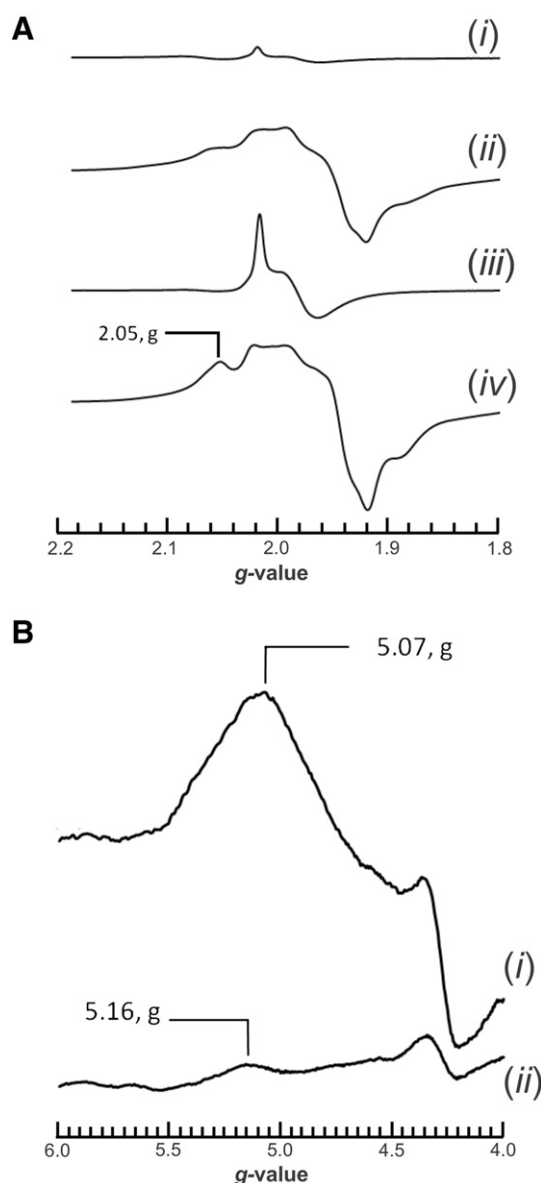
degradation of the entire DmsA-Cys59Ser variant complex: decreased levels of DmsA and DmsB are observed in immunoblots; and negligible amounts of DmsC are detected by fluorescent quench titration. That all three subunits are affected by the DmsA-Cys59Ser substitution is also supported by the absence of the previously-observed lethality effects of DmsC expression in the absence of DmsAB [44,45]: when expressed by itself it uncouples the cytoplasmic membrane and severely inhibits growth on minimal growth media including the glycerol-fumarate medium used herein for protein expression. This is consistent with misfolding of DmsA causing degradation of all three subunits.

In agreement with our earlier observations on the assembly of both DmsABC and NarGHI [20,21], the effect of tungstate on the relative amounts of wild-type enzyme assembled to the cytoplasmic membrane indicates that apomolybdo-enzymes can bypass Mo-bisPGD insertion during maturation. In the case of DmsABC, this results in accumulation of inactive membrane-bound enzyme on the periplasmic side of the membrane [20], consistent with normal translocation of the apomolybdo-DmsAB dimer across the cytoplasmic membrane by the *Tat* translocon, followed by its association with DmsC. This parallels what is observed with NarGHI [40], but with the important difference that the NarGH catalytic dimer is assembled to the inside of the cytoplasmic membrane. Our observations have important implications for the proposed "proofreading" function of the NarJ/DmsD chaperones in that they do not appear to be able to discriminate between apomolybdo- and molydo- forms of the enzyme. In the case of NarGHI, comparison of the structure of the apomolybdo- and molybdo- forms reveals no significant changes in externally-apparent protein structure that the cognate chaperone could use to distinguish between the two enzyme forms [22].

We examined the properties of DmsA-Cys59Ser variant in the presence of molybdate and found the enzyme had wild-type cofactor occupancy, wild-type catalytic activity and it could support anaerobic growth on DMSO. The EPR spectra and redox properties of the Mo and the [Fe–S] clusters in DmsB resembled those of the wild-type. The only observed difference was that the high-spin signal from FS0 appears to be converted to a low-spin signal and only a small fraction was converted from a [4Fe–4S] cluster to a [3Fe–4S] cluster. Taken together these results indicate that a Ser side chain oxygen is able to function as a ligand to FS0 and that the altered cluster is still able to support catalytically-competent rates of electron transfer during enzyme turnover. As is the case with the wild-type enzyme, we were unable to directly determine the reduction potential of FS0 in the DmsA-Cys59Ser variant, but analysis of the potential-dependence of the spin-relaxation of the Mo(V) EPR spectrum suggests that it is lower than -179 mV and significantly lower than that observed by similar measurements in the wild-type enzyme ($E_m = -140$ mV [39]). Broadly similar decreases in reduction potentials of the [4Fe–4S] cluster of *E. coli* fumarate reductase are observed when coordinating Cys residues are replaced with Ser residues [46].

Overall, our results provide new insights into the maturation of CISM enzymes and the interaction between FS0 and Mo-bisPGD and demonstrates that the latter can function as a chemical chaperone during enzyme maturation.

Acknowledgements

References

[1] R.A. Rothery, G.J. Workun, J.H. Weiner, The prokaryotic complex iron−sulfur molybdoenzyme family, Biochim. Biophys. Acta 1778 (2008) 1897–1929.

[2] A. Magalon, J.G. Fedor, A. Walburger, J.H. Weiner, Molybdenum enzymes in bacteria and their maturation, Coord. Chem. Rev. 255 (2011) 1159–1178.

[3] M. Jormakka, S. Törnroth, B. Byrne, S. Iwata, Molecular basis of proton motive force generation: structure of formate dehydrogenase-N, Science 295 (2002) 1863–1868.

[4] M. Jormakka, K. Yokoyama, T. Yano, M. Tamakoshi, S. Akimoto, T. Shimamura, P. Curmi, S. Iwata, Molecular mechanism of energy conservation in polysulfide respiration, Nat. Struct. Mol. Biol. 15 (2008) 730–737.

[5] M.G. Bertero, R.A. Rothery, M. Palak, C. Hou, D. Lim, F. Blasco, J.H. Weiner, N.C.J. Strynadka, Insights into the respiratory electron transfer pathway from the structure of nitrate reductase A, Nat. Struct. Biol. 10 (2003) 681–687.

[6] R.K. Thauer, K. Jungermann, K. Decker, Energy conservation in chemotrophic anaerobic bacteria, Bacteriol. Rev. 41 (1977) 100–180.

[7] S. Leimkühler, M.M. Wuebbens, K.V. Rajagopalan, The history of the discovery of the molybdenum cofactor and novel aspects of its biosynthesis in bacteria, Coord. Chem. Rev. 255 (2011) 1129–1144.

[8] R.J. Turner, A.L. Papish, F. Sargent, Sequence analysis of bacterial redox enzyme maturation proteins (REMPs), Can. J. Microbiol. 50 (2004) 225–238.

[9] S.K. Ramasamy, W.M. Clemons, Structure of the twin-arginine signal-binding protein DmsD from *Escherichia coli*, Acta Crystallogr. Sect. F Struct. Biol. Cryst. Commun. 65 (2009) 746–750.

[10] I.J. Oresnik, C.L. Ladner, R.J. Turner, Identification of a twin-arginine leader-binding protein, Mol. Microbiol. 40 (2001) 323–331.

[11] N.R. Stanley, F. Sargent, G. Buchanan, J. Shi, V. Stewart, T. Palmer, B.C. Berks, Behaviour of topological marker proteins targeted to the Tat protein transport pathway, Mol. Microbiol. 43 (2002) 1005–1021.

[12] M.-R. Yen, Y.-H. Tseng, E.H. Nguyen, L.-F. Wu, M.H. Saier Jr., Sequence and phylogenetic analyses of the twin-arginine targeting (Tat) protein export system, Arch. Microbiol. 177 (2002) 441–450.

[13] F. Blasco, J.P. Dos Santos, A. Magalon, C. Frixon, B. Guigliarelli, C.L. Santini, G. Giordano, NarJ is a specific chaperone required for molybdenum cofactor assembly in nitrate reductase A of *Escherichia coli*, Mol. Microbiol. 28 (1998) 435–447.

[14] A. Vergnes, J. Pommier, R. Toci, F. Blasco, G. Giordano, A. Magalon, NarJ chaperone binds on two distinct sites of the aponitrate reductase of *Escherichia coli* to coordinate molybdenum cofactor insertion and assembly, J. Biol. Chem. 281 (2006) 2170–2176.

[15] H. Li, R.J. Turner, In vivo associations of *Escherichia coli* NarJ with a peptide of the first 50 residues of nitrate reductase catalytic subunit NarG, Can. J. Microbiol. 55 (2009) 179–188.

[16] S. Zakian, D. Lafitte, A. Vergnes, C. Pimentel, C. Sebban-Kreuzer, R. Toci, J.-B. Claude, F. Guerlesquin, A. Magalon, Basis of recognition between the NarJ chaperone and the N-terminus of the NarG subunit from *Escherichia coli* nitrate reductase, FEBS J. 277 (2010) 1886–1895.

[17] D. Sambasivarao, R.J. Turner, J.L. Simala-Grant, G. Shaw, J. Hu, J.H. Weiner, Multiple roles for the twin arginine leader sequence of dimethyl sulfoxide reductase of *Escherichia coli*, J. Biol. Chem. 275 (2000) 22526–22531.

[18] R.A. Rothery, M.G. Bertero, T. Spreter, N. Bouromand, N.C.J. Strynadka, J.H. Weiner, Protein crystallography reveals a role for the FS0 cluster of *Escherichia coli* nitrate reductase A (NarGHI) in enzyme maturation, J. Biol. Chem. 285 (2010) 8801–8807.

[19] H. Tang, R.A. Rothery, J.E. Voss, J.H. Weiner, Correct assembly of iron–sulfur cluster FS0 into *Escherichia coli* dimethyl sulfoxide reductase (DmsABC) is a prerequisite for molybdenum cofactor insertion, J. Biol. Chem. 286 (2011) 15147–15154.

[20] R.A. Rothery, J.L. Grant, J.L. Johnson, K.V. Rajagopalan, J.H. Weiner, Association of molybdopterin guanine dinucleotide with *Escherichia coli* dimethyl sulfoxide reductase: effect of tungstate and a mob mutation, J. Bacteriol. 177 (1995) 2057–2063.

[21] R.A. Rothery, A. Magalon, G. Giordano, B. Guigliarelli, F. Blasco, J.H. Weiner, The molybdenum cofactor of *Escherichia coli* nitrate reductase A (NarGHI) Effect of a mobAB mutation and interactions with [Fe–S] clusters, J. Biol. Chem. 273 (1998) 7462–7469.

[22] R.A. Rothery, M.G. Bertero, R. Cammack, M. Palak, F. Blasco, N.C.J. Strynadka, J.H. Weiner, The catalytic subunit of *Escherichia coli* nitrate reductase A contains a novel [4Fe–4S] cluster with a high-spin ground state, Biochemistry 43 (2004) 5324–5333.

[23] C. Kisker, H. Schindelin, D. Baas, J. Rétey, R.U. Meckenstock, P.M. Kroneck, A structural comparison of molybdenum cofactor-containing enzymes, FEMS Microbiol. Rev. 22 (1998) 503–521.

[24] E. Papp, P. Csermely, Chemical chaperones: mechanisms of action and potential use, in: B.K. Starke, M. Gaestel (Eds.), Molecular Chaperones in Health and Disease, Springer, Berlin Heidelberg, 2006, pp. 405–416.

[25] R.A. Rothery, J.H. Weiner, Alteration of the iron–sulfur cluster composition of *Escherichia coli* dimethyl sulfoxide reductase by site-directed mutagenesis, Biochemistry 30 (1991) 8296–8305.

[26] C.A. Trieber, R.A. Rothery, J.H. Weiner, Multiple pathways of electron transfer in dimethyl sulfoxide reductase of *Escherichia coli*, J. Biol. Chem. 269 (1994) 7103–7109.

[27] D. Sambasivarao, J.H. Weiner, Dimethyl sulfoxide reductase of *Escherichia coli*: an investigation of function and assembly by use of in vivo complementation, J. Bacteriol. 173 (1991) 5935–5943.

[28] C. Condon, J.H. Weiner, Fumarate reductase of *Escherichia coli*: an investigation of function and assembly using in vivo complementation, Mol. Microbiol. 2 (1988) 43–52.

[29] R.A. Rothery, J.H. Weiner, Interaction of an engineered [3Fe–4S] cluster with a menaquinol binding site of *Escherichia coli* DMSO reductase, Biochemistry 35 (1996) 3247–3257.

[30] O.H. Lowry, N.J. Rosebrough, A.L. Farr, R.J. Randall, Protein measurement with the folin phenol reagent, J. Biol. Chem. 193 (1951) 265–275.

[31] M.A. Markwell, S.M. Haas, L.L. Bieber, N.E. Tolbert, A modification of the Lowry procedure to simplify protein determination in membrane and lipoprotein samples, Anal. Biochem. 87 (1978) 206–210.

[32] D. Sambasivarao, D.G. Scraba, C. Trieber, J.H. Weiner, Organization of dimethyl sulfoxide reductase in the plasma membrane of *Escherichia coli*, J. Bacteriol. 172 (1990) 5938–5948.

[33] J.L. Johnson, L.W. Indermaur, K.V. Rajagopalan, Molybdenum cofactor biosynthesis in *Escherichia coli*. Requirement of the chlB gene product for the formation of molybdopterin guanine dinucleotide, J. Biol. Chem. 266 (1991) 12140–12145.

[34] R.A. Rothery, A.M. Seime, A.-M.C. Spiers, E. Maklashina, I. Schröder, R.P. Gunsalus, G. Cecchini, J.H. Weiner, Defining the Q-site of *Escherichia coli* fumarate reductase by site-directed mutagenesis, fluorescence quench titrations and EPR spectroscopy, FEBS J. 272 (2005) 313–326.

[35] G. Van Ark, J.A. Berden, Binding of HQNO to beef-heart sub-mitochondrial particles, Biochim. Biophys. Acta 459 (1977) 119–127.

[36] J.G. Okun, P. Lümmen, U. Brandt, Three classes of inhibitors share a common binding domain in mitochondrial complex I (NADH:ubiquinone oxidoreductase), J. Biol. Chem. 274 (1999) 2625–2630.

[37] Z. Zhao, J.H. Weiner, Interaction of 2-n-heptyl-4-hydroxyquinoline-N-oxide with dimethyl sulfoxide reductase of *Escherichia coli*, J. Biol. Chem. 273 (1998) 20758–20763.

[38] R. Cammack, J.H. Weiner, Electron paramagnetic resonance spectroscopic characterization of dimethyl sulfoxide reductase of *Escherichia coli*, Biochemistry 29 (1990) 8410–8416.

[39] R.A. Rothery, C.A. Trieber, J.H. Weiner, Interactions between the molybdenum cofactor and iron–sulfur clusters of *Escherichia coli* dimethylsulfoxide reductase, J. Biol. Chem. 274 (1999) 13002–13009.

[40] A. Magalon, M. Asso, B. Guigliarelli, R.A. Rothery, P. Bertrand, G. Giordano, F. Blasco, Molybdenum cofactor properties and [Fe–S] cluster coordination in *Escherichia coli* nitrate reductase A: investigation by site-directed mutagenesis of the conserved His-50 residue in the NarG subunit, Biochemistry 37 (1998) 7363–7370.

[41] R.A. Rothery, J.H. Weiner, Topological characterization of *Escherichia coli* DMSO reductase by electron paramagnetic resonance spectroscopy of an engineered [3Fe–4S] cluster, Biochemistry 32 (1993) 5855–5861.

[42] G. Schreiber, A.R. Fersht, Energetics of protein-protein interactions: analysis of the barnase–barstar interface by single mutations and double mutant cycles, J. Mol. Biol. 248 (1995) 478–486.

[43] J.K. Myers, T.G. Oas, Contribution of a buried hydrogen bond to lambda repressor folding kinetics, Biochemistry 38 (1999) 6761–6768.

[44] R.J. Turner, J.L. Busaan, J.H. Lee, M. Michalak, J.H. Weiner, Expression and epitope tagging of the membrane anchor subunit (DmsC) of *Escherichia coli* dimethyl sulfoxide reductase, Protein Eng. 10 (1997) 285–290.

[45] D. Sambasivarao, H.A. Dawson, G. Zhang, G. Shaw, J. Hu, J.H. Weiner, Investigation of *Escherichia coli* dimethyl sulfoxide reductase assembly and processing in strains defective for the sec-independent protein translocation system membrane targeting and translocation, J. Biol. Chem. 276 (2001) 20167–20174.

[46] A.T. Kowal, M.T. Werth, A. Manodori, G. Cecchini, I. Schröder, R.P. Gunsalus, M.K. Johnson, Effect of cysteine to serine mutations on the properties of the [4Fe–4S] center in *Escherichia coli* fumarate reductase, Biochemistry 34 (1995) 12284–12293.